Effect of Iron Ore and Copper Ore Tailings on Engineering Properties and Hydration Products of Sustainable Cement Mortar

E. P. Sumukh [1], B. B. Das[2*], Salim Barbhuiya[3]

[1]Research Scholar, Sustainable Construction and Building Materials Laboratory, Department of Civil Engineering, National Institute of Technology Karnataka, Surathkal, Karnataka, India, 575 025,
Email: sumukh.197cv500@nitk.edu.in

[2]Associate Professor, Department of Civil Engineering, National Institute of Technology Karnataka, Surathkal, Mangaluru - 575 025, India. Email: bdas@nitk.edu.in

[3]Senior Lecturer, Department of Engineering and Construction, University of East London, E16 2RD, United Kingdom. Email: S.Barbhuiya@uel.ac.uk

[*]Corresponding author email: bdas@nitk.edu.in

Highlights

- Fineness of mine tailings played a key role in increasing the performance
- The iron compounds in finer fraction of mine tailings accelerates the hydration
- Secondary hydration reactions were confirmed through advanced characterization.
- The formation of deleterious compounds restricted the high-volume sand replacement.

Abstract

The prohibition of river sand mining has convincingly drawn the research attention in finding the practicable alternatives. In the approach of finding these alternatives, it is essential to ensure a minimal or zero impairment to the ecological balance which can be mainly attained by making use of industrial wastes/by-products. The wastes from the mining industries are the major contributors in causing the impairment to environment, their influence on the stability of mortars on using as fine aggregates need to be systematically investigated with the view of long-term performance concerns.

Thus, the present study explores the applicability of mine tailings and finding the optimum dosage in cement mortars by investigating the engineering properties and microstructure development with the aid of qualitative and quantitative analysis associated to hydration products. The studies confirm that, the increased consumption of portlandite for secondary hydration reactions followed by the additional formation of calcium silicate hydrate (CSH) and calcium aluminum silicate hydrate (CASH) phases in mine tailing-based mortars helped in achieving a quality microstructure. These additional formations of CSH and CASH phases are also confirmed through FTIR by identifying the shift of Si-O-Si stretching vibration bands towards a lower wavenumber. The lowering of Ca/Si atomic ratio and increased formation of mineralogical compounds related to CSH and CASH in XRD patterns also confirms the same. Gismondine, Chabazite and Hillebrandite are the additional phases formed and found to be taken part in refining the pore structure. This enhanced performance of mine tailing mortars was also verified with the aid of modified Andreasen and Andersen particle packing model. The formation of high-quality microstructure is reflected in the hardened properties of optimized cement mortar which in the proportion of 20% for iron ore tailing (IOT) and 30% for copper ore tailing (COT).

Keywords: Mine tailings, mortar, hydration, particle packing, microstructure, characterization, sustainability.

1. Introduction

The ever-increasing quantities of industrial by-products and waste materials produced worldwide, the solid waste management has become a major environmental concern. Discharging industrial wastes such as mine tailings into the environment have a greater ability to cause environmental hazards that can pose a substantial health risk to the creatures. In India, mining industry is one of the most important contributors to the national economy. The principal minerals found in the country include bauxite, chromite, copper, diamond, dolomite, fluorite, graphite, gold, iron ore, limestone etc. Waste materials are generating in abundant quantity during the mining of minerals and ores. Since they are no longer useful to the mine owners, after the extraction of required material, tailings are being dumped in the surroundings which occupy a large amount of land. If not properly maintained, they cause some major hazards to the environment in the form of land degradation, fire hazards, water pollution and air pollution due to the presence of toxic and combustible compositions[1–5]. But maintaining the stability of these dumps is also a major challenge for the mining industry. It has been reported that the quantity of tailings generation went upto 90 – 98% for copper ores and 20 – 50% for other minerals [6–8]. Thus, a huge quantities of tailings are being generated from different sources such as copper ore, bauxite ore, iron ore and gold ore which are estimated to be 4 million tonnes, 2.7 billion tonnes, 290 million tonnes, and 1 tonnes, respectively per annum [9,10].

Due to the lack of landfill space and its high cost, the usage of these mine tailings in some application has become increasingly essential. However, the effective approach for the application of these mine tailings is not being suitably developed[1,2,5]. Thus, there is a potential need to utilize these mine tailings in an effective manner in different fields like construction, pavements, backfilling etc. Whereas on the other hand, river sand mining has been prohibited in many provinces due to the adverse impacts causing ecological imbalances in the environment. But natural river sand has been widely accepted as a conventional fine aggregate in the production of cement mortars. As of now, fine crushed granite rocks (manufactured sand, i.e., M-Sand) have largely replaced the river sand in construction industry. Even though M-Sand showed satisfying performance as an alternative to river sand, it has certain disadvantages in fulfilling the performance requirements of concrete such as grading requirements, workability [11], surface finishing ability [12], compressive strength, density, yield etc. Moreover, the problems associated with the river sand extraction are far more destructive than mining of granite rocks which is being widely accepted as coarse aggregate in producing concrete[13,14]. Thus, the production of concrete and mortars using mine tailings is a best possible option where these tailings can be employed sustainably as an alternative ingredient to river sand. The use of these mine tailings as replacement to conventional materials can not only provide an abundant and cheap source of raw materials for concrete or mortar, but also minimize pollutants and improves the sustainability credentials.

The application of mine tailings as a replacement to river sand in cementitious system has been investigated by the research fraternity and witnessed a satisfactory performance as the mine tailings usually in a well-graded state with its particle size distribution being quite similar to river sand. The previous researches have also revealed that the utilization of mine tailings is economical, efficient, socially beneficial and improves environmental situation[15–18]. The hardened properties of iron ore tailing (IOT) based cementitious composites were reported to be increasing till 25%[19], 25-40%[20], 35%[21], 50%[18] and even for 100%[22] replacement of river sand. Studies have been also reported that density of cementitious composites increases with the usage of mine tailings in the presence of heavy metals[15,18,20,23,24]. However, the workability and durability characteristics were reported to be reducing with the usage of IOT[18–20,22].

The workability characteristics of cementitious composites were found to be enhanced by the usage of copper ore tailing (COT) due to its particle morphology[15]. Previous studies have also witnessed a slight improvement in the hardened properties of COT based cementitious composites till 10-20%[23,24], 60%[25] and even till 100%[26] replacement of river sand. In contrast to this, there is a study claiming the reduced hardened properties with the usage of COT[15]. In addition to these, some studies have also confirmed the reducing durability characteristics by the usage of COT[23,24]. These observed hindrances were primarily attributed to inferior physical properties and grading requirements of mine tailings in comparison with the conventional river sand[15].

However, there observed a great deal of variability in the reported values of engineering properties in the case of cementitious composites produced by using mine tailings. Each of them showed different impact on the mechanical properties and long-term durability of the resulting cement mortar. The influence of using mine tailings followed by the mechanism which alters the engineering properties of cement mortar were not thoroughly investigated in the available literature. In addition, the characterization studies on these mine tailing based cement mortars were found to be very limited in the literature and is need of the hour to understand as it is very much essential in assessing the long-term behavior and to bridge the future research. Hence, the present study aims to comprehensively investigate the influence of using mine tailings as a substitute material to river sand through experimental investigations and characterization techniques. Thus, an attempt has been made to discuss the physical and chemical mechanism that occurs in the cementitious system upon the usage of mine tailings that prerequisite the clear understanding of material, engineering, microstructure and durability properties of cement mortar. Consequently, the present study contributes in developing a sustainable solution for the problems associated with the waste management of copper and iron ore tailings by effectively using them as an alternative to conventional fine aggregates in practice, a way towards achieving sustainability.

2. Materials and experimental methodology

2.1 Materials used and their properties

The binder used for the production of cement mortar was 53 grade ordinary portland cement (OPC 53G) conforming to ASTM C150/C150M-22[27]. Locally available normal potable water conforming to IS 10500:2012 [28] was used for mixing and curing of mortar specimens. Natural river sand falling under zone-II of IS: 383-2016[29] was utilized as fine aggregate and polycarboxylate ether based superplasticizer conforming to IS 2645:2003[30] and IS 9103:1999 [31] was employed to achieve the required flow characteristics in the produced cement mortar. The study mainly highlights the effective utilization of two varieties of mine tailings such as iron ore tailings (IOT) and copper ore tailings (COT) as possible alternatives to river sand.

Various tests were conducted as per the standards to extract the properties of materials used and the observed results are tabulated in Table 1. Fig. 1a) presents their particle size distribution (PSD). The PSD data shows a significant volume of finer fractions (less than 150 microns) were present in mine tailings (11.6% in IOT and 9.9% in COT). The finer fractions of size below 75 microns were found to be 9.4% in COT and 4.8% in IOT. Fig. 1b) presents the XRD patterns of fine aggregates used which highlights their mineralogical compositions and particle geometry. The XRD patterns of river sand show highly crystalline geometry with majorly quartz and traces of copper sulphate and triazene in it. However, the tailing particles showed comparatively more amorphous structure than river sand due to the presence of reactive minerals in them. The lower intensity range of XRD peaks in tailing particles compared to that of river sand confirms the lower crystallinity of mine tailings. The analysis shows that the IOT has aluminosilicate minerals (Al_2SiO_5) such as sillimanite and Kyanite. The iron-based minerals such as coquimbite and Danalite were also detected through XRD analysis. Similarly, the COT shows aluminosilicate minerals such as polylithionite, Anthorite ($CaAl_2Si_2O_8$), chlorite and traces of copper based mineral Mgriite. Similar kind of structural geometry was obtained in the past researches conducted on IOT[19,22] and COT particles[32–34].

The morphology of the tailing particles was studied by conducting SEM under secondary electron mode. Fig. 2 shows the scanning electron micrographs of mine tailings at different magnifications. Table 2 shows the chemical compositions of these mine tailings extracted from X-ray fluorescence spectroscopy (XRF) technique.

Table 1: Properties of various materials used in the study

Properties		**Materials**				
		OPC	**RS***	**IOT**	**COT**	**SP***
Specific gravity		3.11	2.59	3.32	2.39	1.08 ± 0.02
Fineness (m^2/kg)		300	-	-	-	-
Bulk density (kg/m^3)	Loose	-	1500	1733	1372	-
	Compacted	-	1598	1925	1575	-
% of Voids	Loose		43.07	47.71	42.61	-
	Compacted	-	39.34	41.93	34.10	-
Fineness Modulus		-	2.47	2.32	1.74	-
Water absorption (%)		-	0.98	0.66	0.79	-

*- RS: River sand, *SP- Superplasticizer

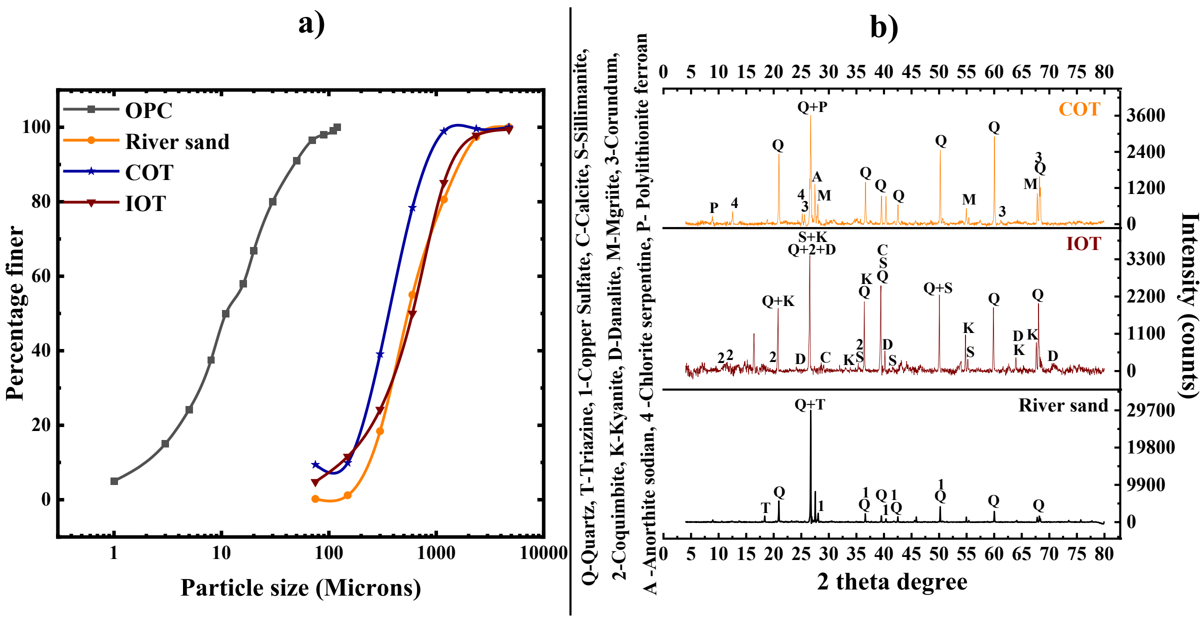

Fig. 1. a) Particle size distribution of various materials used, b) Mineralogical composition of fine aggregates used

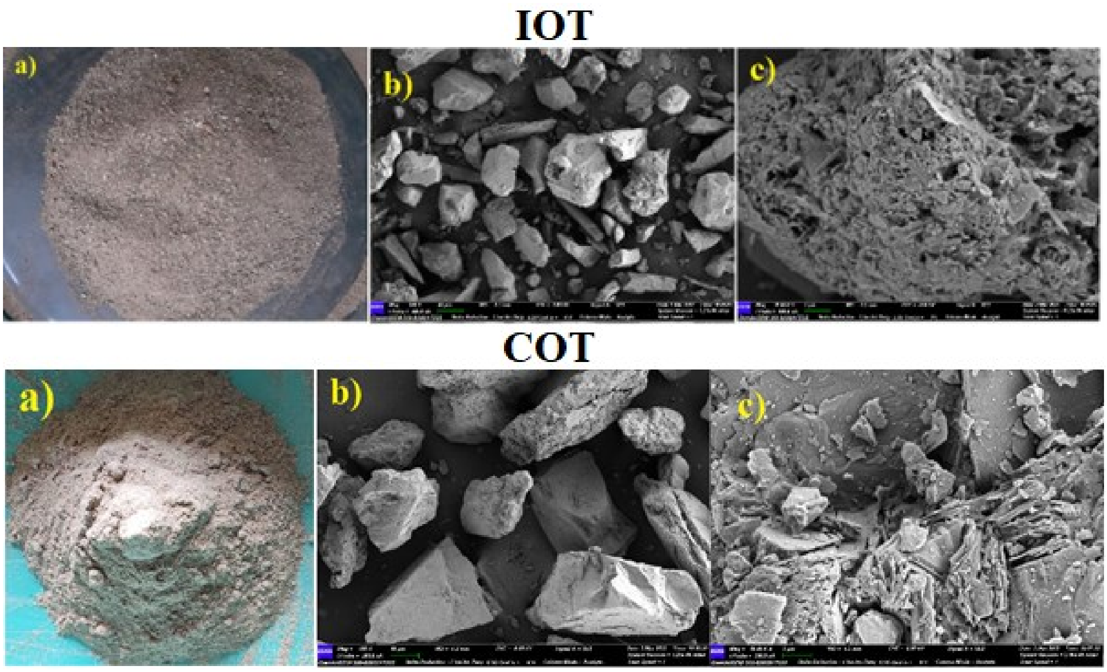

Fig. 2. a) Mine tailing, b) scanning electron micrograph at 500X, c) scanning electron micrograph at 10,000X

Table 2. Chemical compositions of IOT and COT

Component	(% mass)							
	MgO	Al_2O_3	SiO_2	P_2O_5	SO_3	K_2O	CaO	MnO
IOT	1.12	4.54	39.50	0.09	0.09	0.21	0.70	0.31
COT	2.03	8.68	65.26	0.27	4.33	4.12	3.68	0.10
Component	(% mass)							
	Fe_2O_3	Na_2O	Cl	TiO_2	CuO	SrO	ZrO_2	

IOT	53.43	-	-	-	-	-	-
COT	9.65	0.69	0.01	0.64	0.39	0.06	0.07

2.2. Experimental methodology

2.2.1 Details of cement mortar mixes developed

The study was fundamentally carried out with three varieties of cement mortar mixes. Cement mortar produced without any replacement of river sand was considered as reference mix i.e., control mix (CM). The other two varieties of mortar mixes involve the replacement of river sand with mine tailings. The mortar mixes nominated with alphabet "I" belongs to IOT based mortar and with alphabet "C" belongs to COT based mortar. The subsequent numbers represent the replacement level by volume of river sand with mine tailings. All the mortar mixes developed in the study were prepared with water to cement ratio (w/c) of 0.45 and volume of binder to fine aggregate ratio of 1:3. The necessary moisture and water absorption corrections were incorporated while preparing the mortar mixes. To ensure better workability of produced mortar mixes, a minimum flow value of 150 mm was maintained throughout the study using superplasticizer. The detailed mix proportion along with the basic properties of various mortar mixes produced in the present study are being tabulated in Table 3.

Table 3: Details of the mortars produced

Mix name	**Weight (kg/m^3)**				**SP (%)**	**Dry density (kg/m^3)**		**Setting time (mins)**	
	OPC	**RS**	**IOT/ COT**	**Water**		**28 days**	**120 days**	**IST***	**FST***
CM	777.50	1943.25	-	349.88	0.00	2247.82	2273.40	333	448
IOT based mortar									
I10	777.50	1748.93	248.63	349.88	0.09	2259.19	2311.29	288	445
I20	777.50	1554.60	497.25	349.88	0.10	2324.55	2385.17	283	439
I30	777.50	1360.30	745.88	349.88	0.10	2344.44	2387.07	269	423
I40	777.50	1165.95	994.50	349.88	0.25	2356.00	2389.34	227	412
I50	777.50	971.63	1243.13	349.88	0.40	2389.03	2415.49	219	409
COT based mortar									
C10	777.50	1748.93	179.25	349.88	0.00	2279.08	2311.29	304	436
C20	777.50	1554.60	358.50	349.88	0.10	2200.00	2239.30	302	426
C30	777.50	1360.30	537.75	349.88	0.10	2185.00	2225.09	291	420
C40	777.50	1165.95	717.00	349.88	0.10	2119.95	2224.52	275	404
C50	777.50	971.63	896.25	349.88	0.45	2057.43	2207.47	260	399

*bwob-by weight of binder; *IST-initial setting time; *FST-Final setting time

2.2.2 Production of cement mortar samples

Cement mortar specimens of size 70.6 mm × 70.6 mm × 70.6 mm were cast and tested in the present investigation. Mixing of mortar was done in an automatic mortar mixer designed as per the guidelines mentioned in EN 196-1 [35]. The cast specimens were further allowed to set under humid environment (i.e., 27 ± 2°C and 95% RH). Further these specimens were demoulded after 24 hours and immersed in normal potable water for curing maintained at 27 ± 2°C till the date of testing. After the curing period of 3, 7, 28, 56 and 120 days, samples were taken out, dried and tested to check their performance in hardened state.

2.2.3 Details of tests performed

2.2.3.1 Fresh and hardened properties

The mortar mixes were assessed in fresh state to check the workability and setting time. To investigate the hardened properties of produced mortars, tests were carried out using both destructive and non-destructive methods. These tests were conducted at the age of 3, 7, 28, 56 and 120 days of curing for all the mortar mixes. The average of three values obtained from three specimens was taken into consideration and the same was reported. Table 4 shows the details of the tests performed to assess the fresh and hardened properties.

Table 4. Details of the tests conducted to investigate the fresh and hardened properties

Type	Test	Reference	Remarks
Fresh properties	Mini flow table test	EN 1015-3 [36]	-Workability/flowability measurement -To fix the superplasticizer dosage required for maintaining a minimum flow diameter of 150 mm
	Setting time	ASTM C403/C403 M-08 [37]	-Initial and final setting time measurement using Penetration resistance measurements
Hardened properties	Compressive Strength	IS 4031-Part 6:1988 [38]	-Using compressive testing machine at a loading rate of 35 MPa/min
	Dry density	BS EN 1015-10:1999 [39]	-Oven dried weight by volume method using weighing balance
	Permeable porosity	[40,41]	-Vacuum water absorption technique using vacuum desiccators
	Water absorption	ASTM C948 – 81[42]	-Using change in weight at saturated surface dried and oven dried condition

2.3.3.2 Microstructural analysis and characterization techniques used

The performance of cement mortars was primarily influenced by their microstructure. Thus, understanding the microstructure of cement mortars and hydration products formed are very critical. The chunks were collected from the core of mortar samples after 28 and 120 days of curing and kept immersed in isopropyl alcohol for 24 hours to discontinue the hydration mechanism beyond that specific curing age [43,44]. Further the chunks were dried in oven at a temperature range of 40-60 °C till the weight gets stabilized. These oven dried samples were then stored in moist free desiccators maintained using silica gel pellets and vacuum pump. These samples were examined using various characterization techniques to investigate the microstructure development in various types of cement mortars.

a) Scanning electron microscopy and energy dispersive X-Ray spectroscopy (SEM-EDS)

In order to investigate the developed microstructure and to carry out the morphological observations in optimized mortars (best performing), scanning electron microscopy (SEM) technique was used in secondary electron mode. Further, with the aid of energy dispersive X-Ray spectroscopy (EDS), the elemental composition of various types of cement mortars were analyzed. All the preserved samples were gold sputtered before taking them for Microstructural examination.

b) X-Ray diffraction (XRD) analysis

The mineralogical compositions of produced mortars were studied with the help of X-Ray diffraction (XRD) studies. The preserved samples were ground and sieved in 75 microns IS sieve and the collected powdered fine particles were taken for examination. The studies were carried out in Jeol-JPX 8P and Malvern Panalytical make X-ray diffractometers equipped with Cu Ka radiation (40 kV/40 mA) at a scanning rate of 2°/min. The samples were examined with the 2θ angle ranging from 4° to 80° and the received XRD patterns were further analyzed with the aid of software X'Pert High Score Plus.

c) Thermogravimetric analysis (TGA)

Thermogravimetric analysis was performed using RIGAKU TG-DTA 8112 analyzer to quantify the hydration products formed in different types of mortars at 28 days and 120 days of curing age. The hardened paste from the preserved mortar samples were ground in to powder, sieved through 75 µm sieve. The finer powder collected after sieving was characterized in a nitrogen purge environment at temperatures ranging from room temperature to 875°C. The heating rate was maintained at 20°C/min and purge rate was maintained at 20 ml/min. When the hydrated mortar samples were subjected to elevated temperatures, Thermogravimetric mass loss takes place at various different temperature boundaries due to the evaporation of free water, decomposition of hydration products by dehydration, de-hydroxylation and de-carbonation [43,45,46]. These temperature boundaries were determined based on the endothermic peaks formed in derivative thermogravimetric curve (DTG) due to decomposition (weight loss) of compounds. The endothermic peak usually occurs in the temperature range of 50-120°C, 120-150°C, 110-300°C and 230-380°C corresponds to the dehydration of water molecules from the ettringite, gypsum, CSH and friedel's salt, respectively [43,47–52]. Thereafter the weight loss that occurs between 400-500°C is associated to the decomposition of calcium hydroxide (CH) [43,48]. Similarly, the temperature boundary associated to the decomposition of calcium carbonate appears in the temperature boundary of 600-800°C [43].

d) Fourier transform infrared spectroscopy (FTIR)

FTIR studies were performed with the aid of Bruker Alpha II FTIR equipment and OPUS software. The sample preparation is similar to that followed for XRD and TGA analysis. FTIR studies were performed to obtain the transmittance spectra in the wavelength ranges from 600 cm^{-1} to 4000 cm^{-1} under ATR mode. The formation of different phases in cementitious system such as portlanidte ($Ca(OH)_2$), C-S-H, CASH, sulfates and carbonate phases (such as ettringite, hemicarbonate, monosulfoaluminate, sulfoaluminate, calcium carbonate) etc. can be recorded based on the peak intensity and shift over the age of curing and also compared among the different types of mortars produced.

3. Analysis of results and discussions

3.1 Particle packing of the produced cement mortar mixtures

The particle packing of eleven number of mortar mixes designed in the present study were analyzed using modified Andreasen and Andersen packing model [53]. In order to carry out the analysis, "EMMA" software was employed which adopts the principle of modified Andreasen and Andersen packing model. Fig. 3 shows the particle packing curves of mine tailing based mortars. A distribution coefficient (q) of 0.30 appropriate for achieving medium workability was selected for the analysis [43]. From the obtained curves, it is can be clearly observable that the addition of mine tailings improves the particle packing of mortars till a specific replacement level by improving the extent of fitting to the target curve fixed by the modified Andreasen and Andersen packing model for highest particle packing density [54]. Among the various mortar mixes designed, I20 and C30 mixes showed best fitting to the target curve.

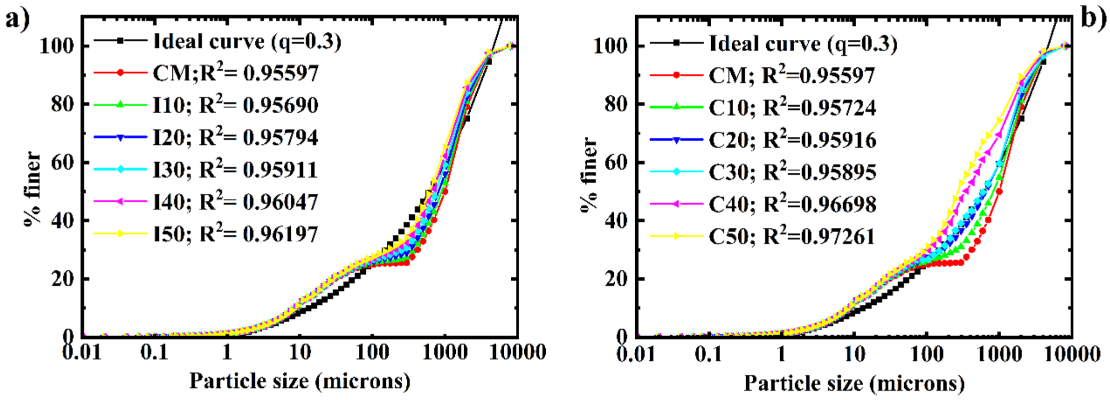

Fig. 3. Particle packing curves of a) IOT based mortars and b) COT based mortars determined using modified Andreasen and Andersen particle packing model

3.2 Fresh properties

3.2.1 Workability

Workability of different types of cement mortar mixes produced using varying dosages of IOT and COT as a replacement to river sand were checked using mini flow table test. To ensure the desired workability in the produced mortar mixes, a minimum flow diameter of 150 mm was fixed and achieved with the aid of superplasticizer. The results reported in the Fig. 4 a) (IOT based mortar) and Fig. 4 b) (COT based mortar) consist of flow diameter, flow value and their corresponding dosage of superplasticizer consumption.

From the obtained results, it can be noticeable that the addition of IOT into the mortar mix as a replacement to river sand reduces the flow characteristics. This behavior can be clearly observed through the dosage of superplasticizer consumption with the percentage usage of IOT. The control mortar (CM) produced entirely with river sand as fine aggregate was observed to achieve required minimum flow diameter of 150 mm without consuming any superplasticizer. With the percentage usage of IOT as replacement to river sand, the flow characteristics were observed to become poorer due to the intrinsic properties of IOT. The rough textured IOT particles increase the friction between the particles and the sharp edges of IOT particles block the movement of particles over one another. Also, the fine nature of IOT particles as compared to river sand leads to filling the void spaces and make the mortar more uniform and cohesive till I20. Further there observed a drastic fall in the flow values (i.e., from I30) which can be attributed to the poor gradational characteristics due to the occurrence of excessive amount of fines which demands higher water content for surface wetting resulting in the formation of stiffer mortar mixes. These observations are in line with the inference made in some past researches[19,20]. The dry and harsh mortar mixes thus produced leads to increased superplasticizer consumption to a greater extent and thereby mortar mixes showed reduced workability.

Similarly in the COT based mortar, a sudden drop in the flow values were observed beyond 30% replacement of river sand with COT due to the increased amount of fines in the mortar mix. This can be clearly observed through the flow values and the superplasticizer dosages consumed among the mixes C30, C40 and C50. Even though the superplasticizer dosage was kept constant between the mixes C30 and C40, there observed a sudden declination in the flow values and further from C40 to C50 mix, there observed a sudden increment in the superplasticizer dosage requirement. However, the flow characteristics were found to be improved right from the CM and till C30. This can be clearly noticeable from the flow values and their corresponding superplasticizer dosage from CM to C10 and C20 to C30 mix. This behavior can be attributed to the smooth glossy textured and angular shaped COT particles reduce the friction and helps in movement among the particles with great ease[25,26]. Also, the fine particles of COT initially tend to fill the voids at lower replacement levels (till 30%) and make the mixes uniform and cohesive that helped in improving the flow characteristics[15].

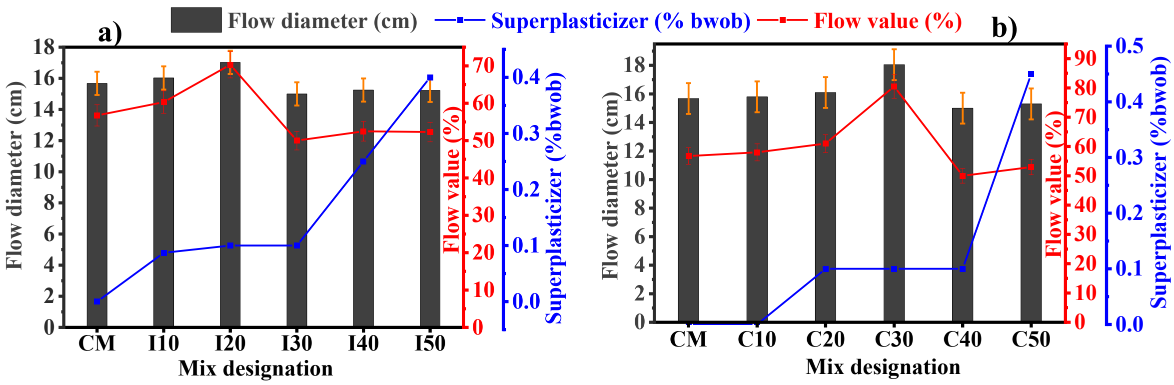

Fig. 4. a) Flow characteristics of a) IOT based mortar; b) COT based mortar

3.3 Hardened properties

3.3.1 Compressive strength

Compressive strength development in control (CM), mine tailing based mortars were measured at the curing age of 3, 7, 28, 56 and 120 days and the results are plotted as histogram. Fig. 5 a) and Fig. 5 b) presents the compressive strength of IOT based and COT based mortars, respectively.

The results obtained from both IOT and COT based mortars exhibited a decreasing trend with the content of mine tailings in the initial days of curing (i.e., 3 days and 7 days). Even though mine tailings accelerated the hydration reaction leading to early setting of mortar (Table 3), they exhibited slightly lower compressive strength at early ages of curing till 7 days. This reduction in the compressive strength with the increasing amount of mine tailings is due to the slowing down of hydration reaction by the development of low permeability layer of heavy metals around the non-hydrated cement grains[55,56]. The presence of Cu ions also slightly delays the hydration process due to the precipitation of oxides and hydroxides[56–60]. However there observed a significant improvement in the compressive strength development of mine tailing based mortars with the progress in curing age (beyond 7 days of curing). This could be attributed to the acceleration in the hydration activity of cement particles under the influence reactive minerals present in tailings. The presence of iron compounds at higher concentrations in the mortar accelerates the hydration process[19,57,58,61,62]. The additional calcium content added from the finer fractions of mine tailings also contributes in accelerating the hydration process[57,58]. The IOT based mortars showed an increasing trend of compressive strength till a sand replacement level of 20% and COT based mortars till a sand replacement level of 30%. The improved particle packing and thereby improvised particle packing density of the mortar mixes with the addition of IOT till 20% and COT till 30% helped the ingredients of mortar to undergo primary and possible secondary hydration reactions more effectually[19,63]. Since the mine tailings are rich in siliceous and aluminous compounds, the finer fractions of mine tailings facilitate in undergoing supplementary hydration reactions (secondary hydration reaction/ pozzolanic reaction) after 7 days of curing resulting in the formation of additional hydration products[19].

The dry density results presented in Table 3 also evident the occurrence of secondary hydration reaction. The difference between the dry densities of mine tailing based mortars with the percentage replacement of sand was found to be reducing with the progress in curing age which is attributed to the formation of additional hydration products by the finer fractions of tailings through secondary hydration reactions. These actions helped in refining the pore structure of mortars in an effective manner leading to the formation of dense microstructure that enhances the hardened mechanical properties such as compressive strength. It is also important to notice from the results that the compressive strength of the mortars reduces beyond the optimized dosage of mine tailings which is due to the effect from poorer gradational characteristics and excessive silica-alumina content that restrains the degree of hydration reactions. Similar trend of compressive strength of mortar by the usage of IOT & COT in relation to control mortar was observed in the past literatures[18–20,23–25]. The percentage strength gain of I20 mortar was recorded to be 2.55%, 13.75% and 20.53% at the curing age of 28, 56 and 120 days respectively. Similarly, C30 mortar exhibits 29.17%, 6.20% and 17.08% at 28, 56 and 120 days of curing age respectively.

3.3.2 Water absorption and Permeable porosity

The water absorption and permeable porosity of control and mine tailing based mortars were assessed at the end of 3, 7, 28, 56 and 120 days of curing. Fig. 5 c) and Fig. 5 d) presents the water absorption of IOT based and COT based mortars respectively. Similarly, Fig. 5 e) and Fig. 5 f) represents the permeable porosity of IOT based and COT based mortars respectively. The results obtained shows that both water absorption and permeability porosity follow a quite similar trend with the percentage usage of mine tailings at all the curing ages. This could be due to the fact that the absorbed water predominantly accumulates in the permeable void spaces or pores present in the mortar mixes and these pore volumes are usually regarded as porosity. It is also important to notice that both water absorption and permeable porosity reduces with the progress in curing age which is due to the formation and accumulation of hydration products that refines the pore structure in mortar.

The utilization of mine tailings in the mortars as a replacement to river sand showed positive results in the case of water absorption and permeable porosity. The water absorption and permeable porosity were found to be reducing with the increasing proportion of mine tailings till certain replacement level and thereafter found to be increasing. This behavior can be ascribed to the improved particle packing and improved affinity to undergo secondary hydration reaction by the finer fractions of mine tailings with the increasing level of sand replacement[19,63]. Similar trend of reducing water absorption with the usage of IOT was noticed by previous studies[19]. The mortar mixes “I20” and “C30” recorded lowest water absorption and permeable porosity values. In addition to these, the lower water absorbing capacity of IOT and COT in comparison with the river sand also contributes in reducing the water absorption and permeable porosity of mortar. However, exceeding the dosage of mine tailings beyond optimum percentage (i.e., 20% of IOT and 30% of COT) causes an increase in the water absorption and permeable porosity due to poor gradational characteristics and lack in water availability for undergoing hydration reactions caused by the increased amount of fines in the mortar mix. The reduced alkalinity in the mortar by the high-volume replacement of sand by mine tailings might also be the cause for the increased water absorption and permeable porosity.

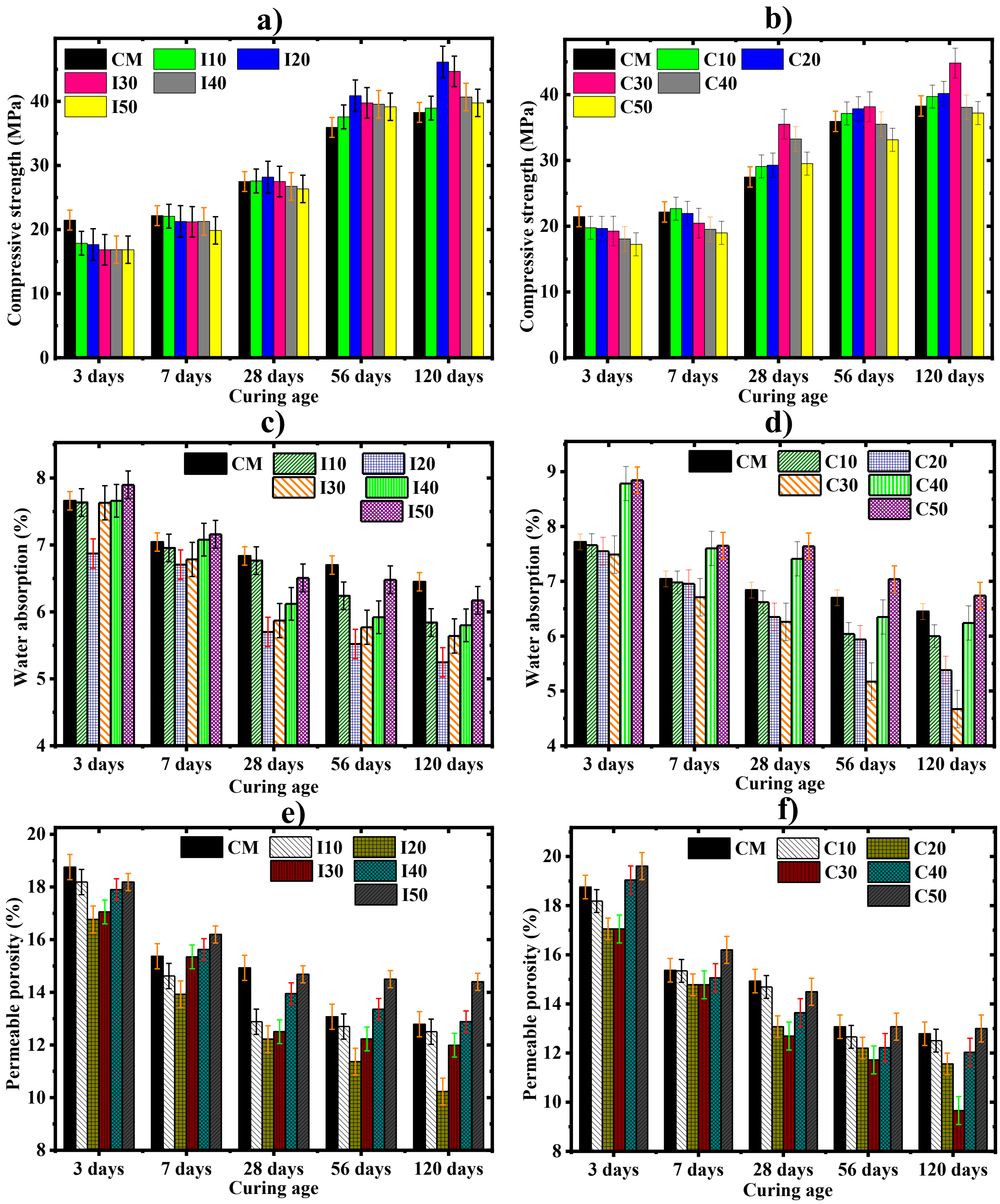

Fig. 5. a) Compressive strength, c) Water absorption, e) permeable porosity of IOT based mortars, and b) Compressive strength, d) Water absorption, f) Permeable porosity of COT based mortars

3.4 Microstructure and characterization studies

3.4.1 Mineralogical characterization

The influence of different dosages of mine tailings on the mineralogical compounds was studied at the curing age of 28 days and 120 days using the XRD patterns. The XRD analysis was carried out for the control mortar, and till one replacement level beyond the optimum mine tailing-based mortar (i.e., till I30 and C40). The details of the mineralogical compounds such as chemical name, empirical formula, peak assignment designations were tabulated in Table 5.

Fig. 6 a) presents the XRD patterns of 28 days cured and Fig. 6 b) presents XRD patterns of 120 days cured mortar samples of the optimized mixes (i.e., CM, I20 and C30). By observing the XRD patterns of 28 days cured mortar samples, it can be noticeable that the crystalline phases are more and prominent in mine tailing based mortars due to the presence of more CH and other unhydrated particles in comparison with the control mortar. The occurrence of portlandite (CH) peaks are more and prominent in mine tailing-based mortars which is due to additional portlandite formed from the calcium particles present in the finer fraction of mine tailings[57,58]. The increased portlandite peaks is also due to accelerated hydration reaction caused by improved particle packing intensity and higher iron oxide compounds[57,58,61–63]. In addition to these, there observed a preferential formation of additional calcium silicate hydrates (CSH) and calcium silicate aluminum hydrate (CASH) phases due to the occurrence of effective primary and secondary hydration reactions facilitated by the finer fraction of mine tailings. The mineralogical compounds related to CSH and CASH phases such as Gismondine, Chabazite, Xonotlite and Hillebrandite were found to be additionally formed.

However, by observing the XRD patterns of 120 days cured mortar samples, it can be noticeable that the XRD patterns of mine tailing based mortars appeared more amorphous than 28 days ones and also in comparison with the control mortar. This is attributed to the effective conversion of crystalline CH to amorphous gel like structure formed by CSH and CASH phases through primary and secondary hydration reactions. The produced CH in control mortar remained mostly unutilized after 28 days of curing. Whereas, the portlandite produced in the mine tailing-based mortars were appeared to get consumed for secondary hydration reactions. The formation of additional hydration phases related to CSH and CASH are evident for the consumption of portlandite in mine tailing-based mortars. The mineralogical compounds related to CSH and CASH phases such as Gismondine, Chabazite, Wairakite, Hillebrandite and Tobermorite were found to be additionally formed which helped in refining the pore structure of mine tailing based cement mortar. In addition, the occurrence of various phases of carbonates, gypsum and ettringites are also the cause for more crystalline XRD patterns in control mortar.

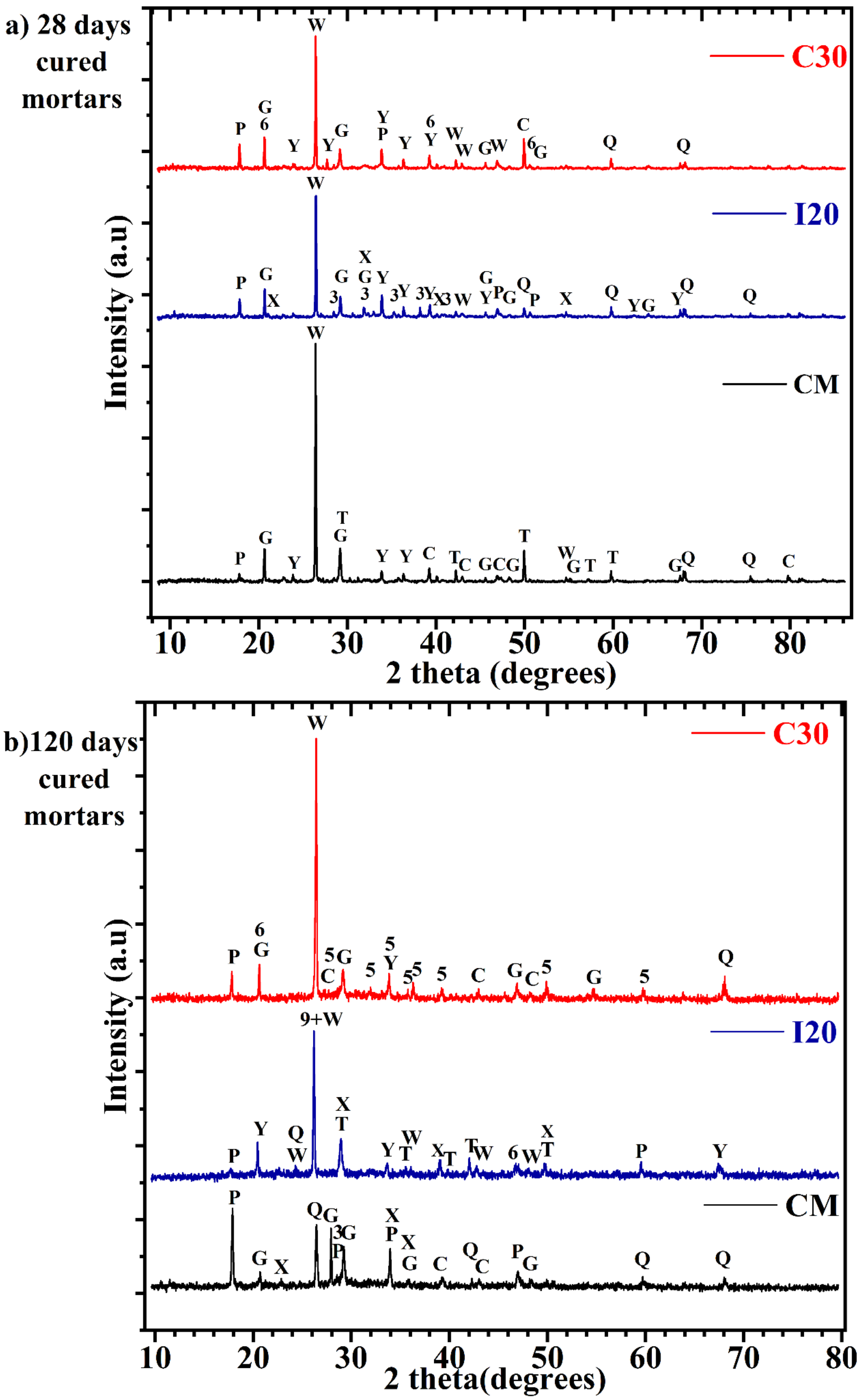

a) 28 days cured mortars
C30
I20
CM
Intensity (a.u)
2 theta (degrees)
10
20
30
40
50
60
70
80
b)120 days cured mortars
C30
I20
CM
9+W
Intensity (a.u)
2 theta(degrees)

Fig. 6. XRD pattern of optimized mortars at the curing age of a) 28 days and b) 120 days

Overall, by observing the XRD patterns, there can be seen that more mineralogical compounds related to calcium silicates and calcium aluminum silicates were formed with lesser carbonates, gypsum and ettringite phases by the utilization of mine tailings in cement mortar. This development in mine tailing mortars helped to perform superior than the control mortar. This enhanced performance can also be witnessed through the measured engineering properties such as compressive strength, water absorption and permeable porosity.

Table 5. Details of the mineralogical compounds and their peak assignment

Compound details	Peak assignment of COT based mortar										Peak assignment of IOT based mortar					
	28 days curing					120 days curing					28 days curing			120 days curing		
	CM	**C10**	**C20**	**C30**	**C40**	**CM**	**C10**	**C20**	**C30**	**C40**	**I10**	**I20**	**I30**	**I10**	**I20**	**I30**
Quartz (Silicon Oxide) (SiO_2)	Q	Q	Q	Q	Q	Q	Q	Q	Q	Q	Q	Q	Q	Q	Q	Q
Portlandite (Calcium Hydroxide) ($Ca(OH)_2$)	P	P	P	P	P	P	P	P	P	P	P	P	P	P	P	P
Hillebrandite (Calcium Silicate Hydroxide) ($Ca_2(SiO_3)(OH)_2$)			2		2								2			2
Kamaishilite ($Ca_2Al_2SiO_6(OH)_2$) (Calcium Aluminium Silicate Hydroxide)		3				3					3	3				
Tobermorite ($Ca_5(OH)_2Si_6O_{16}\cdot 4H_2O$) (Calcium Silicate Hydroxide Hydrate)	T														T	
Xonotlite (Calcium Silicate Hydrate) ($Ca_6Si_6O_{17}(OH)_2$)			X		X	X	X			X	X	X		X	X	
Calcium Silicate Hydrate ($Ca_2SiO_4\cdot H_2O$)			5				5	5	5							
Chabazite ($Ca_2Al_4Si_8O_{24}\cdot 12H_2O$) (Calcium Aluminum Silicate Hydrate)				6	6				6						6	
Wairakite ($CaAl_2Si_4O_{12}\cdot 2H_2O$) (Calcium Aluminum Silicate Hydrate)	W			W					W			W			W	
Gismondine ($CaAl_2Si_2O_8.4H_2O$) (Calcium Aluminium Silicate Hydrate)		7	7				7	7		7	7		7	7		7
Calcite (Calcium Carbonate) ($CaCO_3$)	C	C	C	C	C	C	C	C	C	C	C		C	C		C
Gypsum (Calcium Sulfate Hydrate) ($CaSO_4.2H_2O$)	G			G	G	G	G	G	G		G	G	G		G	
Yeelimite (Calcium Aluminum Oxide Sulfate) ($Ca_3Al_6O_{12}.CaSO_4$)	Y			Y					Y	Y		Y		Y	Y	

3.4.2 Thermogravimetric analysis (TGA) on IOT and COT based cement mortar

From the thermogravimetric analyzer, the weight loss of the mortar samples with the increasing temperature was recorded and for the analysis TG/DTG curves were plotted. Fig. 7 a) and Fig. 7 b) presents the TG/DTG curves of 28 days and 120 days cured IOT based mortar samples, respectively. Similarly, Fig. 7 c) and Fig. 7 d) shows the TG/DTG curves of 28 days and 120 days cured COT based mortar samples, respectively.

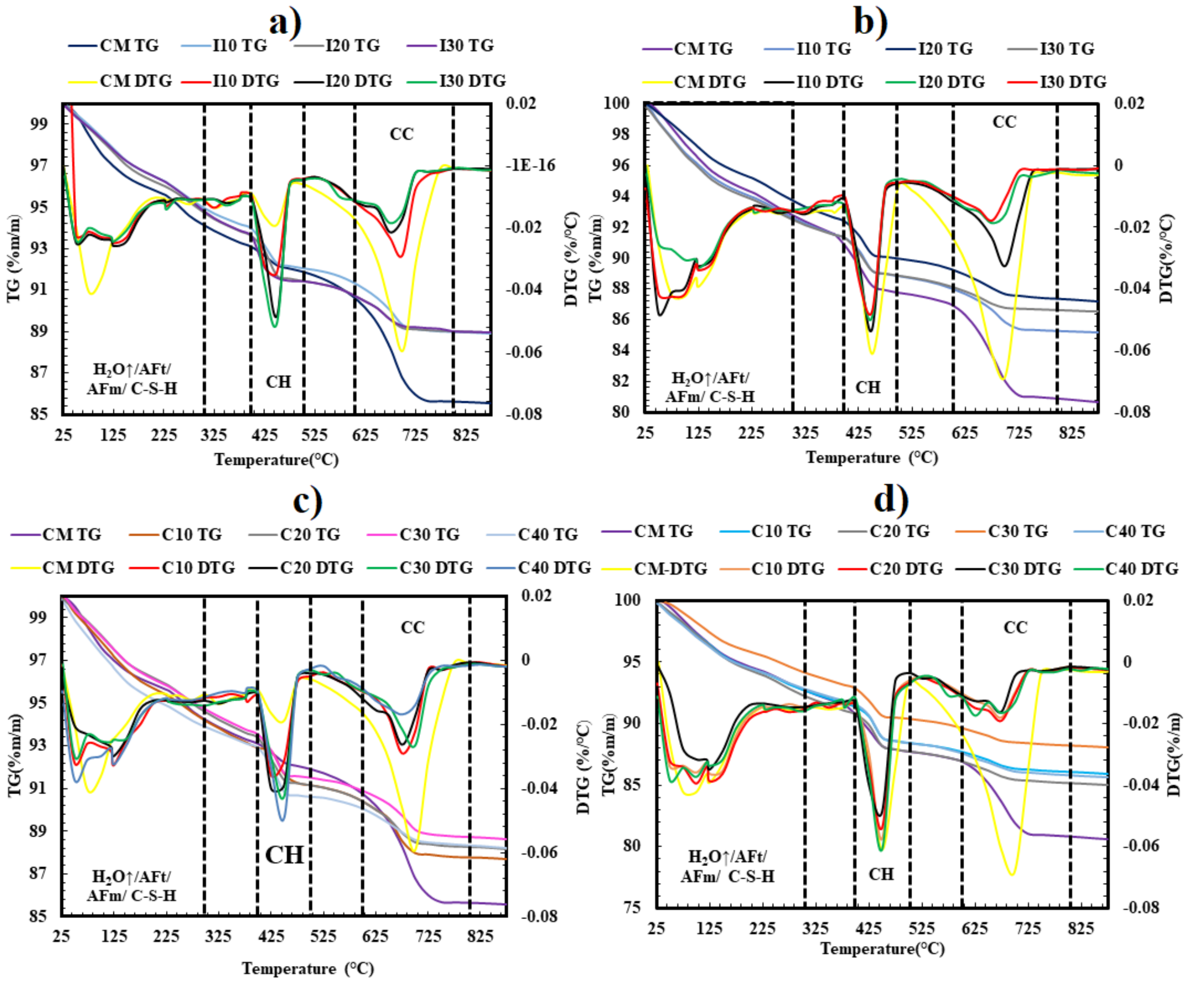

Fig. 7. TG and DTG curves of a) IOT based mortar after 28 days of curing, b) IOT based mortar after 120 days of curing, c) COT based mortar after 28 days of curing and d) COT based mortar after 120 days of curing

In the present study, the hydration products such as calcium hydroxide (CH) and calcium carbonate (CC) were quantified on the basis of their decomposition by weight loss at their specific temperature boundaries. The various other hydration products such as gypsum, ettringite, CSH, CASH, friedels salts etc. were not computed in the present study due to the overlapping among the respective temperature boundaries [43,49,50]. The quantified values of CH and CC are graphically represented in Fig. 8.

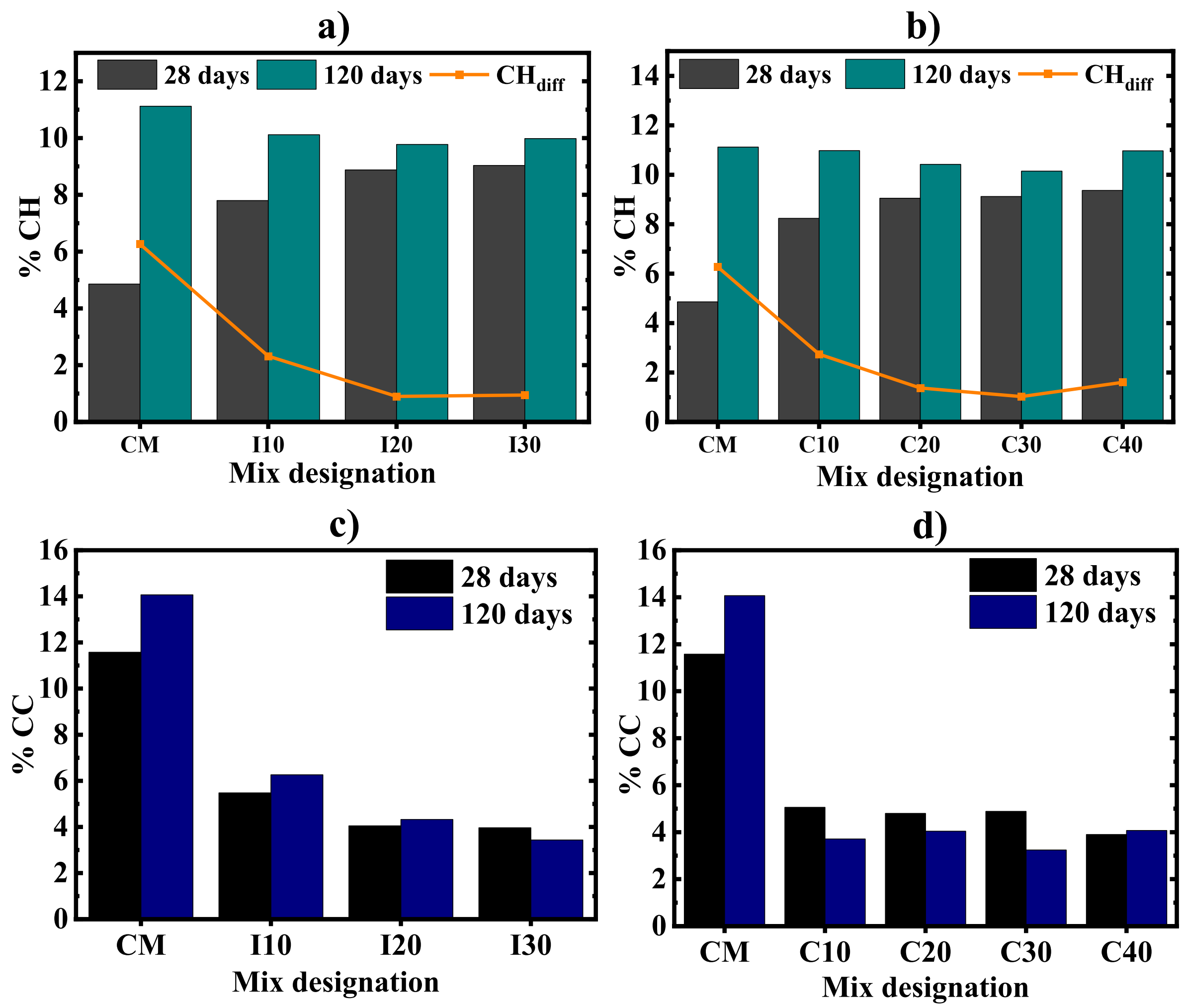

Fig. 8. Phase compounds formed in IOT based mortar [(a) CH; (c) CC] and COT based mortar [(b) CH; (d) CC] after 28 days and 120 days of curing

The TGA results of 28 days cured IOT and COT based mortar samples shows an increasing CH content with the increasing percentage of river sand replacement by mine tailings. This is attributed to the accelerated hydration reaction due to enhanced particle packing density and participation of elements of iron, i.e., Fe^{+} generated from the finer fractions of mine tailings[19,57,58,61,62]. In addition to this, the additional CaO added from the mine tailings also marginally contributes to the generation of CH[57,58]. Meanwhile, there will be some influence of heavy metals and copper ions too. The heavy metals present in mine tailings create a low permeability layer around the particles which delays the hydration reaction[55,56]. The presence of Cu ions also slightly delays the hydration process due to the precipitation of oxides and hydroxides[56–60]. The delayed hydration reaction thus slowdowns the consumption of CH for further reactions which creates a higher CH reserve in the mine tailing-based mortars pore solution. The improved particle packing caused by the finer particle size distribution of mine tailings also leads to the extensive formation of CSH/CASH gels along with higher volume of portlandite[57,58,61–63].

Apart from these, mine tailing based mortars recorded lower content of CC which can be seen in Fig. 8 where the control mortar showed highest amount of CC. It is also essential to notice that there is a preferential formation of ettringite in the control mortar which can be seen by an intensive endothermic peak in DTG curve. However, the mine tailing-based mortar showed comparatively wider but less intense endothermic peak which is evident for the lesser formation of gypsum and ettringite.

By observing the DTG curves and quantified CH values corresponding to 120 days cured samples, it can be seen that the generation of CH continues with the curing age in all types of mortars. Whereas the consumption of CH for the secondary hydration reactions was found to be significantly more in mine tailing based mortars which can be seen from the reducing trend of CH_{diff} (difference between the CH values at 28 and 120 days curing) shown in Fig. 8. Conversely the endothermic peaks corresponding to CSH and CASH were found to be broadened and intensified with the curing age which signifies the effective formation of CSH and CASH gels in mine tailings based mortars. It is also important to note that the consumption of CH is slightly more in the optimized mine tailing based mortar (i.e. I20 and C30) which is due to the optimized mine tailing percentage favorable for undergoing reactions and superior particle packing that might helped in undergoing the reactions efficiently. The quantified values of CC by the end of 120 days of curing also shows the presence of CC in lower volume in mine tailing based mortars. Thus, the additionally formed CSH/CASH gels along with the lower content of CC, ettringite and gypsum ensures better performance in the case of mine tailing based mortars.

3.4.3 Fourier transform infrared spectroscopy (FTIR)

Fig. 9 a) and Fig. 9 b) illustrates the FTIR spectra of IOT based cement mortar at the curing age of 28 days and 120 days respectively. Similarly, Fig. 10 a) and Fig. 10 b) illustrates the FTIR spectra of COT based cement mortar at the curing age of 28 days and 120 days respectively. The corresponding details about the functional group assignment for various wavenumbers are presented in Table 6.

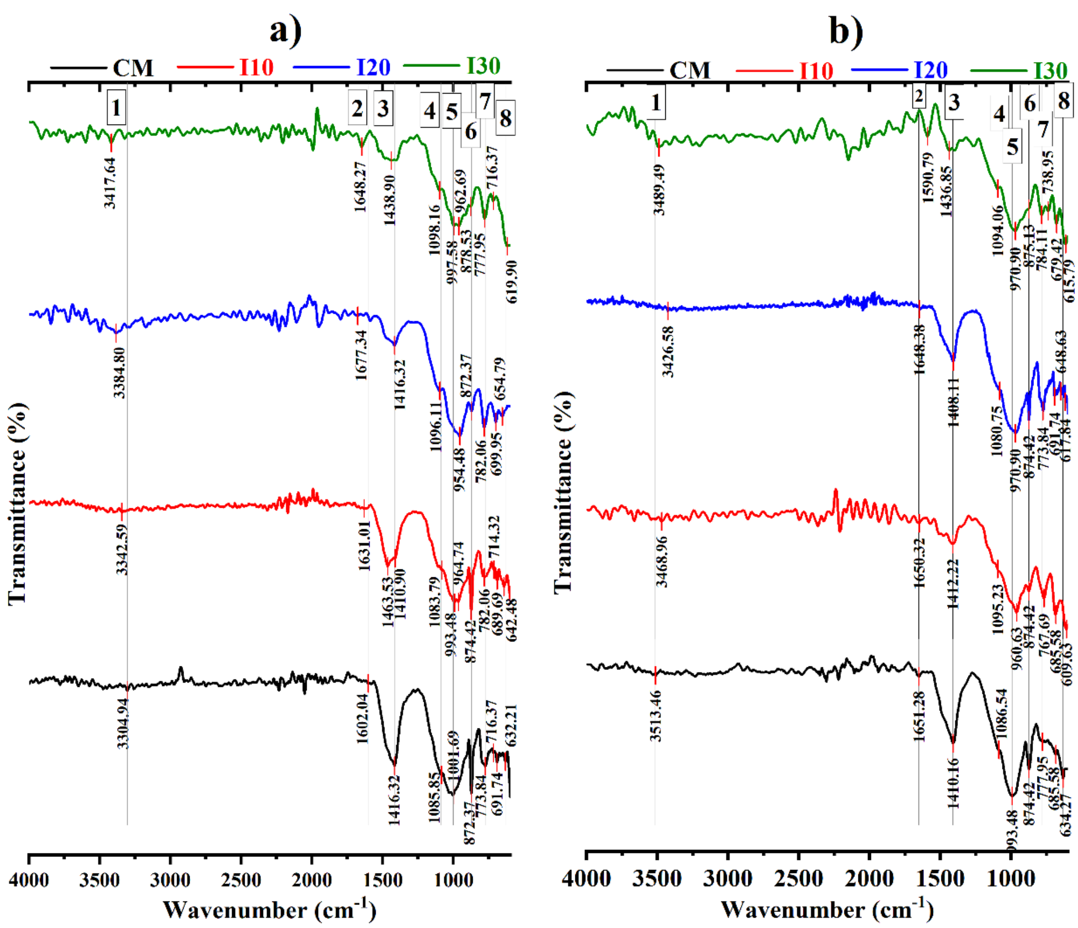

Fig. 9. FTIR spectra of control and IOT based mortar samples at a) 28 days of curing and b) 120 days of curing

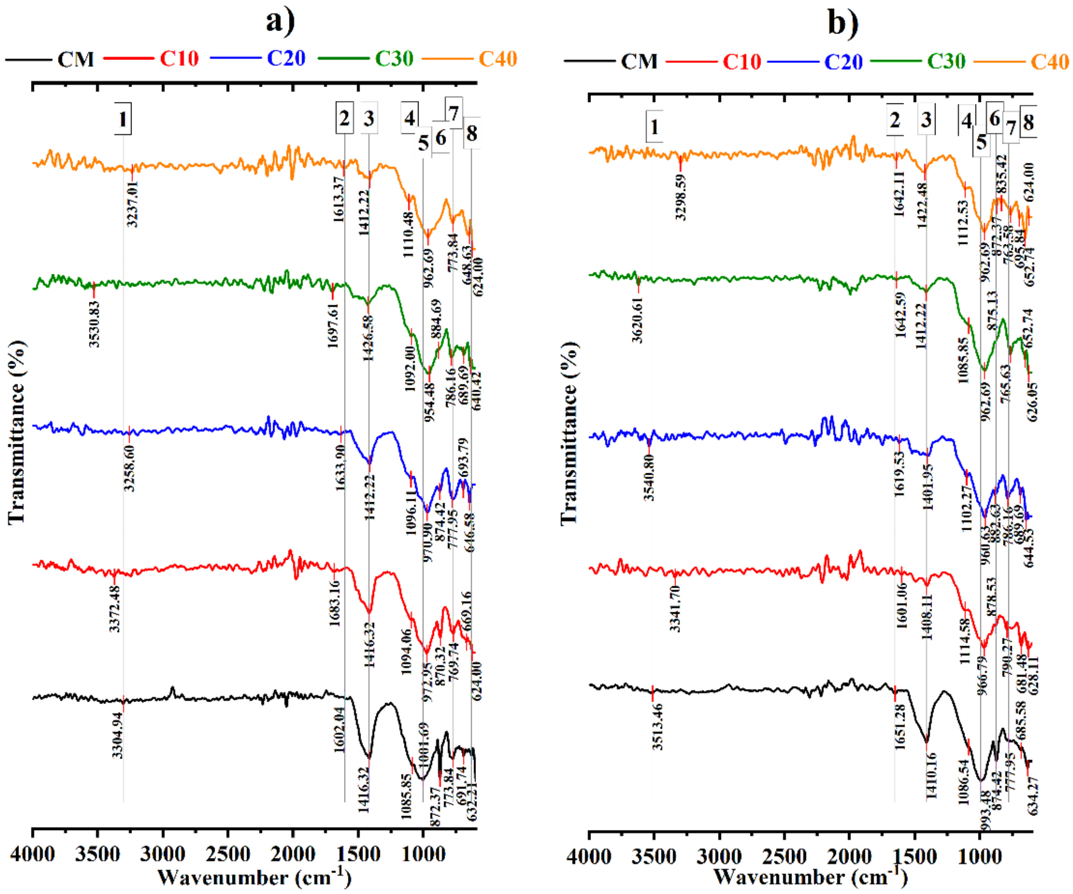

Fig. 10. FTIR spectra of control and COT based mortar samples at a) 28 days of curing and b) 120 days of curing

It can be observed from the FTIR spectra's that the vibration bands and the corresponding functional groups assigned were found to be same in all the types of mortars (i.e., CM, IOT based and COT based mortar) both at 28 days and 120 days of curing. By observing the FTIR spectra's, it can be noticeable that the vibration band corresponding to Si-O-Si asymmetric stretching found in the wavenumber range of 1000 cm^{-1} is more prominent in control mortar and optimized mine tailing mortars (i.e., I20 and C30). These vibration bands were found to be more intense and broader than the rest of the mine tailing based mortars[64–66]. This could be attributed to the uninterrupted hydration reactions occurred in CM and effective hydration reactions taken place under the effect of superior particle packing along with the presence of iron oxides mine tailings, that facilitated in the generation of higher amount of CSH gels[63]. The occurrence of secondary hydration reactions facilitated by the finer fractions of mine tailings also generates additional C-S-H phases.

For brevity, the wavenumbers corresponding to Si-O-Si/Al asymmetric stretching were color scaled from red to green in Table 6, where red represents the highest, green represents the lowest and yellow represents the wavenumber that exists between the highest and lowest. By observing the wavenumbers corresponding to Si-O-Si/Al asymmetric stretching band, there observed a change in color scale from red to green by the utilization of mine tailings which signifies the decrease in wavenumbers from 1001.68 cm^{-1} to 954.48 cm^{-1} in 28 days cured mortars and from 993.48 cm^{-1} to 960.63 cm^{-1} in 120 days cured mortars. The decrease in wavenumber of Si-O-Si/Al asymmetric stretching band signifies the change of microstructure followed by the formation of more amorphous products with stronger bonds due to the additional formations of silicates and aluminosilicate hydrates[67–70]. It is also important to note that the I10 and I30 mortars showed additional peaks at wavenumbers 993.48cm^{-1} and 997.58 cm^{-1} respectively which is evident for the formation of additional C-S-H phases by the intrusion of IOT in mortar.

The vibration band associated to Si-O-Si/Al symmetric stretching were found to be more prominent in mine tailing-based mortars both at 28 days and 120 days of curing. Especially in the case of 120 days cured samples, the vibration bands corresponding to Si-O-Si/Al symmetric stretching were found to be comparatively broader and intense than that of control mortar. This is mainly ascribed to the formation of additional CSH and CASH phases through the effective hydration reactions facilitated by the improved particle packing achieved from the fine nature of mine tailings[63]. The finer fractions of mine tailings also contribute in the additional formation of CSH and CASH gels through secondary hydration reactions. The additional peak found at the wavenumber 738.95 cm^{-1} could be due to the formation of additional C-S-H/CASH phases by the intrusion of IOT in mortar. All these observations are found to be in good alignment with the XRD analysis data.

By observing the color scales, there is also a considerable shift of Si-O-Si/Al symmetric stretching bands towards the lower wavenumber by the inclusion of mine tailings. This fact gives the information that stronger bonds were developed by the formation of additional CSH and CASH phases in mine tailing based mortars[67–70]. It is also important to notice that there is no significant shift observed in the wavenumbers associated to the Si-O-Si/Al symmetric stretching by the inclusion of mine tailing by the end of 28 days of curing. This could be due to the negligible amount or absence of secondary hydration reactions at the early stages of curing by the delayed hydration activity caused by the heavy metals[55,56].

However, there also observed a drastic reduction in the intensities of vibration bands corresponding to O-C-O asymmetric stretching and O-C-O bending with the usage of mine tailings in both 28 days 120 days cured mortar samples. This behavior is attributed to the increased compactness in the mine tailing based mortars owing to accelerated hydration activity that leads to the formation of additional CSH and CASH gels, which acts as carbonation barrier[71]. This feature helped the mine tailing-based mortars to have an advanced quality microstructure even though the hydration reactions lagged in the early stages of curing. These observations are in good alignment with the TGA and SEM studies.

Table 6: Details of the functional group assignment at different wavenumbers

Notation No	Age of curing	Wavenumber (cm^{-1}) corresponding to different peaks								Functional group assignment
		CM	I10	I20	I30	C10	C20	C30	C40	
1	28	3305	3343	3385	3418	3372	3259	3531	3237	O-H asymmetric stretching (Due to bonded water in portlandite and free water)
	120	3513	3469	3427	3489	3342	3541	3621	3299	
2	28	1602	1631	1677	1648	1683	1634	1698	1613	O-H asymmetric bending (Due to free water)
	120	1651	1650	1648	1591	1601	1620	1643	1642	
3	28	1416	1464	1416	1439	1416	1412	1427	1412	O-C-O asymmetric stretching (Due to carbonates)
	120	1410	1412	1408	1437	1408	1401	1412	1422	
4	28	1086	1084	1096	1098	1094	1096	1092	1110	S-O stretching (Due to gypsum and ettringites)
	120	1087	1095	1081	1094	1115	1102	1086	1113	
5	28	-	993	-	998	-	-	-	-	Si-O-Si/Al asymmetric stretching (Due to silicates and aluminosilicate hydrates)
		1002	965	954	963	973	971	954	963	
	120	993	961	971	971	967	961	963	963	
6	28	872	874	872	879	870	874	885	-	O-C-O bending (Due to carbonates)
	120	874	874	874	875	879	883	875	872	
7	28	774	782	782	778	770	778	786	774	Si-O-Si/Al symmetric stretch (Due to silicates and aluminosilicate hydrates)
		716	714	-	716	-	-	-	-	
		692	689	699	-	-	693	689	-	
	120	778	767	773	784	790	786	765	763	
		-	-	-	738	-	-	-	-	
		686	685	691	679	681	689	-	695	
8	28	632	642	655	620	669	647	640	649	S-O bending (Due to gypsum and ettringites)
		-	-	-	-	624	-	-	624	
	120	634	610	618	616	628	645	653	653	
		-	-	-	-	-	-	626	624	

3.4.4 Scanning electron microscopy (SEM) and energy dispersive x-ray spectroscopy (EDS)

The morphology and the microstructure of hydrated samples of control, optimized IOT and COT mortars (i.e., CM, I20 and C30) were studied using SEM at the curing age of 28 days and 120 days. Fig. 11 and Fig. 12 depicts the scanning electron micrographs of 28 days and 120 days cured mortar samples, respectively. The compounds in the micrographs were visually identified based on their structure, shape, color and texture[72]. Further the elemental composition of these mortar samples was investigated using area method in EDS technique. The Ca/Si atomic ratio was calculated from the obtained results and tabulated in Table 7. It was used to examine the extent of formation of major products related to hydration such as calcium hydroxide (CH) and CSH. Numerous researches have claimed that the formation of CSH through hydration process highly depends on the calcium (Ca) and silicate (Si) ions present in the pore solution [72–74]. It has been reported that the cement matrix having lower Ca/Si atomic ratio signifies to have a dense microstructure owing to the formation of strongly built CSH network [75,76].

By observing the SEM micrographs of 28 days cured samples, it is possible to notice that the mine tailings-based mortars developed additional portlandite, CSH and CASH phases from to the accelerated hydration reactions facilitated by the superior particle packing, added calcium oxide and iron oxide compounds from the finer fractions of mine tailings[57,58,61,62]. The increased Ca/Si ratio in mine tailing-based mortars is evident for the increased formation of portlandite. However, the extensive formation of CSH and CASH phases in mine tailing-based mortars helped in achieving a quality microstructure which is responsible for the improved hardened properties.

Similar kind of observations can also be made in 120 days cured mortar. But the scanning electron micrographs were found to have much more CSH and CASH phases due to the succession of hydration reactions with the curing age. As depicted in the SEM micrographs, the iron ore tailing based mortar showed globular, needled like and amorphous network of CSH and CASH phases. Whereas, floccular, fibrous and plate like structured CSH and CASH phases were formed in COT bases mortars. These diversely formed CSH and CASH phases beyond 28 days of curing in the mine tailing-based mortars are evident for the formation of additional hydration products through secondary hydration reactions, facilitated by the reactive finer fractions present in mine tailings. The reduction in Ca/Si atomic ratio in mine tailings mortar at the end of 120 days curing was also significantly higher than control mortar due to the effective utilization of CH for secondary hydration reactions. It is also important to notice that the occurrence of higher volume of CC and ettringites can also be observed only in the SEM images of control mortar. Whereas the mine tailing-based mortars illustrates less CC and ettringites with ample amount of CSH and CASH.

Thus, the additional hydration products formed from the primary and secondary hydration reactions helps in densifying the mortar microstructure which steer the mine tailings-based mortars to perform better than conventional mortar.

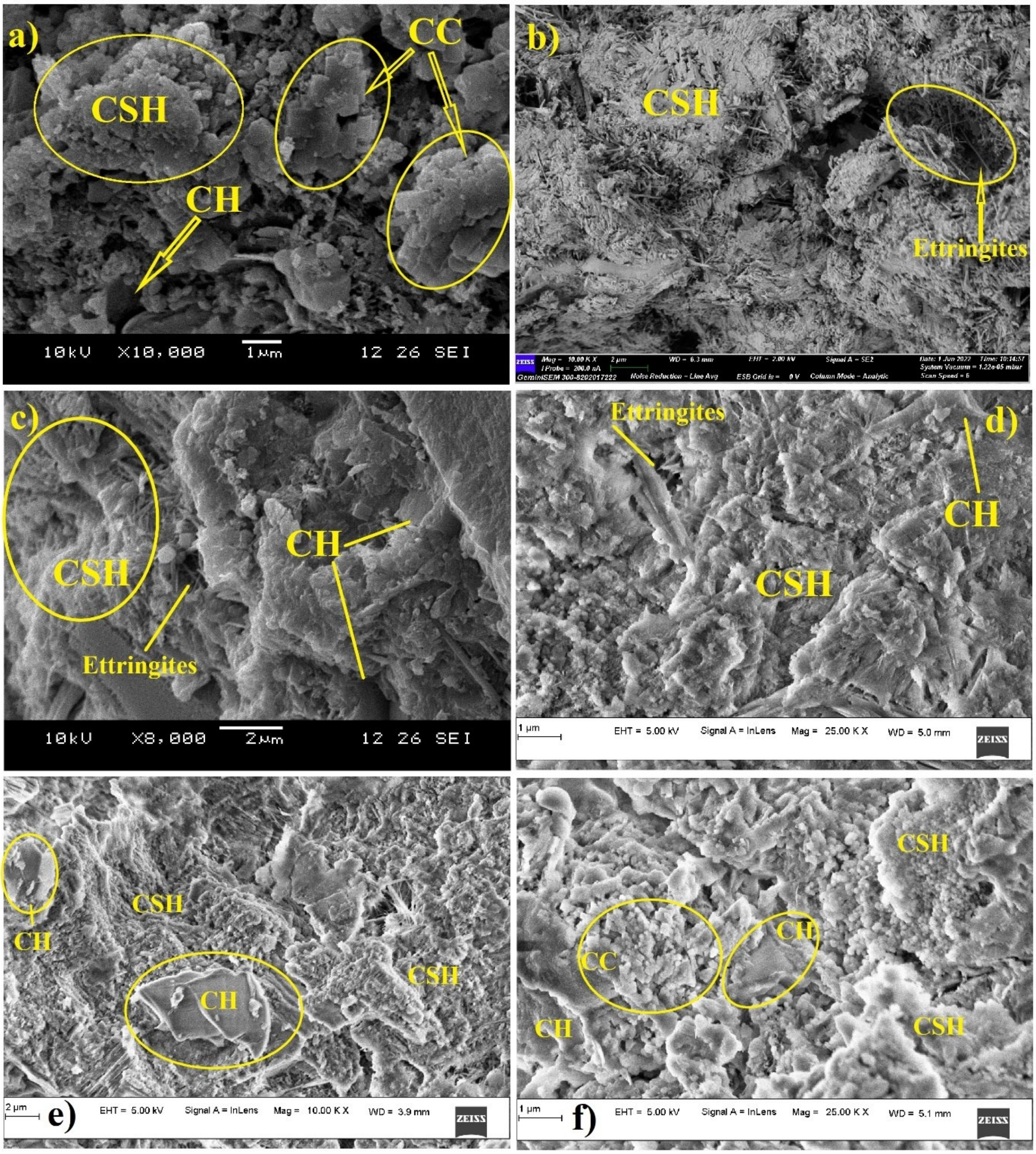

Fig. 11. Scanning electron micrograph of control (CM) [in a), b)], I20 [in c), d)] and C30 [in e), f)] mortar at 28 days of curing.

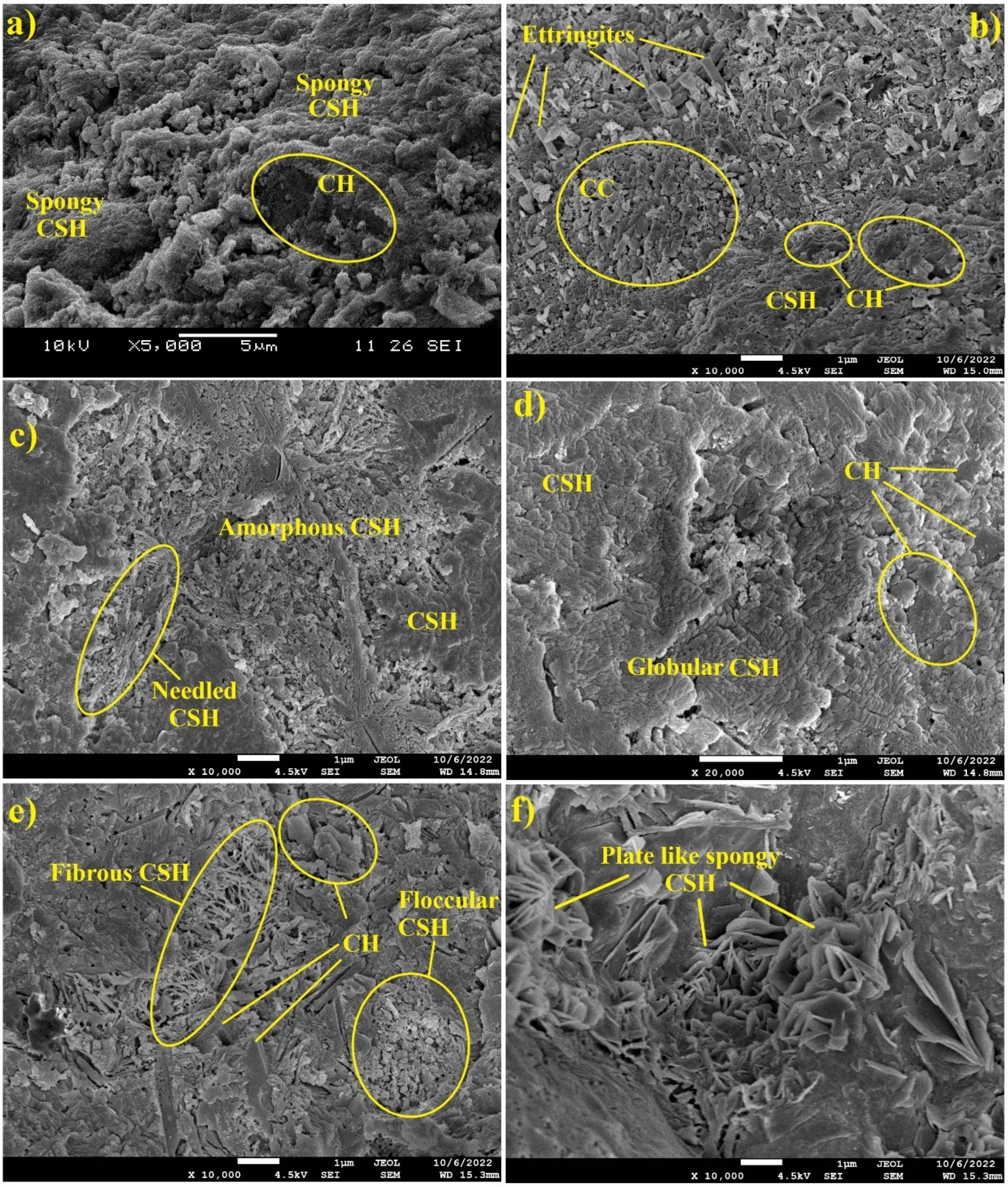

Fig. 12. Scanning electron micrograph of control (CM) [in a), b)], I20 [in c), d)] and C30 [in e), f)] mortar at 120 days of curing.

Table 7: EDS elemental analysis of control, IOT and COT based mortars after a curing period of 28 days and 120 days

Element	Atomic weight (%) of 28 days cured mortar			Atomic weight (%) of 120 days cured mortar		
	CM	I20	C30	CM	I20	C30
C	15.43	14.04	15.38	10.00	12.05	17.05
Ca	21.20	20.97	20.96	9.85	15.70	10.90

O	54.79	55.69	55.48	60.60	50.90	51.05
Al	0.22	0.75	0.81	2.55	0.95	3.40
Si	7.475	6.9	6.28	4.05	6.60	5.50
Mg	0.16	0.14	0.18	-	0.25	0.05
S	0.28	0.28	0.28	10.65	3.35	0.75
Cl	0.03	0.05	0.02	-	-	-
K	0.11	0.08	0.13	0.30	0.60	1.80
Fe	0.3	1.1	0.48	1.75	1.55	0.10
Na	-	-	0.21	0.25	0.05	0.65
P	-	-	-	-	3.10	-
Mn	-	-	-	-	4.80	1.45
Ti	-	-	-	-	-	0.30
Zr	-	-	-	-	-	1.45
Ca/Si	**2.83675**	**3.03913**	**3.33758**	**2.432**	**2.378**	**1.98198**

4. Conclusions

After analyzing the experimental results in detail, the following conclusions can be drawn,

- The preliminary investigations on the mine tailings used in the present study revealed that they have comparable properties with the river sand and hence could be used as an alternative to river sand in developing the cementitious composites.
- The fresh properties such as workability and setting time reduce with the inclusion of mine tailings as a replacement to river sand. The present study confirms the requirement of superplasticizer and recommends desired volumes of superplasticizer (about 0-0.45% by weight of binder) for achieving the required flow of 150 mm in different mortars mixes.
- The improved particle packing by the inclusion of mine tailings till certain replacement level of river sand helped in improving the hardened properties of mortar such as compressive strength, water absorption and permeable porosity. However, the dry density of mortars greatly relies on the specific gravity of tailings used.
- The outcome from the characterization studies such as lowering of Ca/Si ratio in EDS, formation of additional CSH and CASH peaks in XRD, increased consumption of CH observed in TGA and occurrence of broad, intensive Si-O-Si/Al stretching bands with considerable shifts towards lower wavenumber in FTIR studies confirms the occurrence of secondary hydration reactions by the finer fractions of mine tailings which helped in improving the microstructure (can be observed through SEM images) and overall performance (compressive strength, water absorption and permeable porosity) of the cement mortar.
- The study concludes that, 20% of IOT and 30 % of COT by volume of river sand can be considered as a potential replacement level for achieving superior performance in cement mortar.
- By the end of 120 days of curing, I20 showed 20.53% higher compressive strength, 4.92% higher dry density, 1.20% lower water absorption and 2.56% lower permeable porosity than the control mortar. Similarly, C30 showed 17.08% higher compressive

strength, 2.17% lower dry density, 1.78% lower water absorption and 3.13% lower permeable porosity.

- Fineness of the material, angular particle shape along with the presence of higher concentration of silica and alumina in the finer fractions of COT played a key role in achieving the higher level of replacement for copper ore tailings in comparison with iron ore tailings.
- The rough textured fine particles of IOT along with higher concentration of Fe_2O_3, helped in achieving higher density and better performance in iron ore tailing based mortar.

Declaration of Competing Interest

The authors declare that they have no conflict of interest, financial interests or personal relationships that could have appeared to influence the research work reported in this article.

References

1. J. R. Owen, D. Kemp, É. Lébre, K. Svobodova, and G. P. Murillo, "Catastrophic tailings dam failures and disaster risk disclosure," *International journal of disaster risk reduction* 42, (January 2020):101361, https://doi.org/10.1016/j.ijdrr.2019.101361.

2. F. F. Carmo, A. O. Lanchotti, and L. H. Y. Kamino, "Mining waste challenges: environmental risks of gigatons of mud, dust and sediment in megadiverse regions in Brazil," *Sustainability* 12, no. 20 (October 2020): 8466, https://doi.org/10.3390/su12208466.

3. W. Pytel, "Risk assessment of mine tailings/waste surface ponds," in *Mine Waste 2010: Proceedings of the First International Seminar on the Reduction of Risk in the Management of Tailings and Mine Waste*, (2010): 229–242, https://doi.org/10.36487/ACG_rep/1008_20_Pytel.

4. Z. Różański, "Fire hazard in coal waste dumps–selected aspects of the environmental impact," in *IOP Conference Series: Earth and Environmental Science* 174, no. 1 (2018): 12013, DOI 10.1088/1755-1315/174/1/012013.

[5] C. Cacciuttolo, D. Cano, and M. Custodio, "Socio-Environmental Risks Linked with Mine Tailings Chemical Composition: Promoting Responsible and Safe Mine Tailings Management Considering Copper and Gold Mining Experiences from Chile and Peru," *Toxics*, vol. 11, no. 5, p. 462, 2023.

[6] D. P. Mohapatra and D. M. Kirpalani, "Process effluents and mine tailings: sources, effects and management and role of nanotechnology," *Nanotechnology for Environmental Engineering*, vol. 2, no. 1, pp. 1–12, 2017, doi: 10.1007/s41204-016-0011-6.

[7] C. Falagán, B. M. Grail, and D. B. Johnson, "New approaches for extracting and recovering metals from mine tailings," *Minerals Engineering*, vol. 106, pp. 71–78, 2017, doi: 10.1016/j.mineng.2016.10.008.

[8] H. R. Watling, "Review of biohydrometallurgical metals extraction from polymetallic mineral resources," *Minerals*, vol. 5, no. 1, pp. 1–60, 2014, doi: 10.3390/min5010001.

[9] Geological Survey of India, "Government of India Ministry of Mines REPORT OF THE

WORKING GROUP ON (OTHER THAN COAL & LIGNITE) THE TWELFTH FIVE YEAR PLAN SUB GROUP – I," 2011.

[10] Indian Bureau of Mines, "Part-I: General Reviews," *Indian Mineral Yearbook 2012*, vol. 2012, no. 0712, pp. 1–7, 2014.

[11] C. Sudha, A. K. Kottuppillil, P. T. Ravichandran, and K. Divya Krishnan, "Study on Mechanical Properties of Concrete with Manufactured Sand and Bagasse Ash," *Indian Journal of Science and Technology*, vol. 9, no. 34, 2016, doi: 10.17485/ijst/2016/v9i34/95867.

[12] M. Pilegis, D. Gardner, and R. Lark, "An investigation into the use of manufactured sand as a 100% replacement for fine aggregate in concrete," *Materials*, vol. 9, no. 6, 2016, doi: 10.3390/ma9060440.

[13] W. H. Langer and B. F. Arbogast, "Environmental impacts of mining natural aggregate," *Deposit and geoenvironmental models for resource exploitation and environmental security*, pp. 151–169, 2002.

[14] L. H. Anh *et al.*, "Life Cycle Assessment of River Sand and Aggregates Alternatives in Concrete," *Materials*, vol. 16, no. 5, p. 2064, 2023.

[15] F. Muleya, B. Mulenga, S. L. Zulu, S. Nwaubani, C. K. Tembo, and H. Mushota, "Investigating the suitability and cost-benefit of copper tailings as partial replacement of sand in concrete in Zambia: an exploratory study," *Journal of Engineering, Design and Technology*, vol. 19, no. 4, pp. 828–849, 2021.

[16] A. Bandopadhyay, R. Kumar, and P. Ramachandrarao, "Clean technologies for metallurgical industries (EWM-2002)," 2002.

[17] S. Zhang *et al.*, "Current situation and comprehensive utilization of iron ore tailing resources," *Journal of mining Science*, vol. 42, pp. 403–408, 2006.

[18] A. U. Shettima, Y. Ahmad, M. W. Hussin, N. Z. Muhammad, and O. E. Babatude, "Strength and microstructure of concrete with iron ore tailings as replacement for river sand," in *E3S web of conferences*, 2018, vol. 34, p. 1003.

[19] A. U. Shettima, M. W. Hussin, Y. Ahmad, and J. Mirza, "Evaluation of iron ore tailings as replacement for fine aggregate in concrete," *Construction and Building Materials*, vol. 120, pp. 72–79, 2016.

[20] S. Oritola, A. L. Saleh, and A. R. Mohd Sam, "Performance of iron ore tailings as partial replacement for sand in concrete," *Applied Mechanics and Materials*, vol. 735, pp. 122–127, 2015.

[21] Z. Tian, Z. Zhao, C. Dai, and S. Liu, "Experimental study on the properties of concrete mixed with iron ore tailings," *Advances in Materials Science and Engineering*, vol. 2016, 2016.

[22] Z. Zhang, Z. Zhang, S. Yin, and L. Yu, "Utilization of iron tailings sand as an environmentally friendly alternative to natural river sand in high-strength concrete: shrinkage characterization and mitigation strategies," *Materials*, vol. 13, no. 24, p. 5614, 2020.

[23] R. C. Gupta, P. Mehra, and B. S. Thomas, "Utilization of copper tailing in developing sustainable and durable concrete," *Journal of Materials in Civil Engineering*, vol. 29,

no. 5, p. 4016274, 2017.

[24] B. S. Thomas, A. Damare, and R. C. Gupta, “Strength and durability characteristics of copper tailing concrete,” *Construction and Building Materials*, vol. 48, pp. 894–900, 2013.

[25] A. M. Bhoi, Y. D. Patil, H. S. Patil, and M. P. Kadam, “Feasibility assessment of incorporating copper slag as a sand substitute to attain sustainable production perspective in concrete,” *Advances in Materials Science and Engineering*, vol. 2018, pp. 1–11, 2018.

[26] K. S. Al-Jabri, M. Hisada, A. H. Al-Saidy, and S. K. Al-Oraimi, “Performance of high strength concrete made with copper slag as a fine aggregate,” *Construction and building materials*, vol. 23, no. 6, pp. 2132–2140, 2009.

[27] ASTM C150/C150M-22, “Standard Specification for Portland Cement,” *ASTM C150/C150M-22*, no. Reapproved 1999, pp. 1–9, 2003, doi: 10.1520/C0150.

[28] BIS, “Indian Standard Drinking Water Specification (Second Revision),” *Bureau of Indian Standards*, vol. IS 10500, no. May, pp. 1–11, 2012, [Online]. Available: http://cgwb.gov.in/Documents/WQ-standards.pdf

[29] BIS (Bureau of Indian Standards), “Coarse and Fine Aggregate for Concrete-Specification IS 383:2016,” *New Delhi, India: BIS*. pp. 1–21, 2016.

[30] Bureau of Indian Standards, “IS 2645: 2003 Integral Waterproofing Compounds for Cement Mortar and Concrete -Specification,” p. 16, 2003.

[31] I. 9103-1999, “Indian standard concrete admixtures-specifications.” Bureau of Indian Standards New Delhi.

[32] X. Tian, H. Zhang, T. Zhang, and C. A. Fernández, “Alkali-activated copper tailings-based pastes: Compressive strength and microstructural characterization,” *Journal of Materials Research and Technology*, vol. 9, no. 3, pp. 6557–6567, 2020.

[33] L. Cui, L. Wang, Y. Xu, X. Lou, and H. Wang, “Feasibility Evaluation of Replacing River Sand with Copper Tailings,” *Sustainability*, vol. 13, no. 14, p. 7575, 2021.

[34] B. S. Jain, “Green Geopolymers with Copper Tailings for Marine Environments,” pp. 1–8, 2022.

[35] B. S. EN, “1052-3. BS EN 196-1: Methods of testing cement,” *Determination of strength*, 2005.

[36] B. S. EN, “1015-3. Methods of Test for Mortar for Masonry—Part 3: Determination of Consistence of Fresh Mortar (by Flow Table),” *NBN, Bureau for Standardisation: Brussels, Belgium*, 1999.

[37] ASTM C403, “ASTM C 403, ‘Standard Test Method for Time of Setting of Concrete Mixtures by Penetration Resistance,’ ASTM C 403-95, Annual Book of ASTM Standards, American Society for Testing and Materials, Pennsylvania, 1998. ASTM,” pp. 1–7, 2005, doi: 10.1520/C0403.

[38] I. S. IS, “Indian Standard Is: 4031 (Part 6)-1988 (Reaffirmed 2005). Methods Of Physical Tests For Hydraulic Cement Part 6 Determination Of Compressive Strength Of Hydraulic Cement Other Than Masonry Cement (First Revision),” 2005.

[39] B. S. EN, "1015-10, 1999. Methods of test for mortar for masonry—Part 10: Determination of dry bulk density of hardened mortar," *Br. Stand.[29] BS EN*, pp. 1011–1015, 1999.

[40] M. Safiuddin and N. Hearn, "Comparison of ASTM saturation techniques for measuring the permeable porosity of concrete," *Cement and Concrete Research*, vol. 35, no. 5, pp. 1008–1013, 2005.

[41] B. B. Das, D. N. Singh, and S. P. Pandey, "A comparative study for determining pore volume of concrete," *Indian Concrete Journal*, vol. 84, no. 12, p. 7, 2010.

[42] A. ASTM, "Standard test method for dry and wet bulk density, water absorption, and apparent porosity of thin sections of glass-fiber reinforced concrete," *ASTM C948-81*, 2016.

[43] K. Snehal, B. B. Das, and M. Akanksha, "Early age, hydration, mechanical and microstructure properties of nano-silica blended cementitious composites," *Construction and Building Materials*, vol. 233, p. 117212, 2020.

[44] J. Zhang and G. W. Scherer, "Comparison of methods for arresting hydration of cement," *Cement and Concrete Research*, vol. 41, no. 10, pp. 1024–1036, 2011.

[45] J. W. Bullard *et al.*, "Mechanisms of cement hydration," *Cement and concrete research*, vol. 41, no. 12, pp. 1208–1223, 2011.

[46] R. Yu, P. Spiesz, and H. J. H. Brouwers, "Effect of nano-silica on the hydration and microstructure development of Ultra-High Performance Concrete (UHPC) with a low binder amount," *Construction and Building Materials*, vol. 65, pp. 140–150, 2014.

[47] L. Soriano, J. Monzó, M. Bonilla, M. M. Tashima, J. Payá, and M. V Borrachero, "Effect of pozzolans on the hydration process of Portland cement cured at low temperatures," *Cement and Concrete Composites*, vol. 42, pp. 41–48, 2013.

[48] L. P. Singh, A. Goel, S. K. Bhattacharyya, U. Sharma, and G. Mishra, "Hydration studies of cementitious material using silica nanoparticles," *Journal of Advanced Concrete Technology*, vol. 13, no. 7, pp. 345–354, 2015.

[49] K. Snehal and B. B. Das, "Acid, alkali and chloride resistance of binary, ternary and quaternary blended cementitious mortar integrated with nano-silica particles," *Cement and Concrete Composites*, vol. 123, p. 104214, 2021.

[50] K. Snehal and B. B. Das, "Pozzolanic reactivity and drying shrinkage characteristics of optimized blended cementitious composites comprising of Nano-Silica particles," *Construction and Building Materials*, vol. 316, p. 125796, 2022.

[51] K. Snehal, B. B. Das, and S. Barbhuiya, "Influence of aggressive exposure on the degradation of nano-silica admixed cementitious mortar integrated with phase change materials," *Construction and Building Materials*, vol. 335, p. 127467, 2022.

[52] K. Snehal and B. B. Das, "Effect of phase-change materials on the hydration and mineralogy of cement mortar," *Proceedings of the institution of civil engineers-construction materials*, pp. 1–11, 2020.

[53] D. R. Dinger and J. E. Funk, "Particle-packing phenomena and their application in materials processing," *Mrs Bulletin*, vol. 22, no. 12, pp. 19–23, 1997.

[54] C. Emma and S. Distribution, "EMMA User Guide Version 1 User Guide Elkem Materials Mixture Analyser-EMMA", [Online]. Available: www.elkem.com

[55] M. Gou, L. Zhou, and N. W. Y. Then, "Utilization of tailings in cement and concrete: A review," *Science and Engineering of Composite Materials*, vol. 26, no. 1, pp. 449–464, 2019.

[56] D. Boakye and H. Uzoegbo, "Assessment of concrete with pulverized copper slag as partial replacement of cement," *Concr. Beton*, vol. 139, pp. 14–17, 2014.

[57] M. Yellishetty, V. Karpe, E. H. Reddy, K. N. Subhash, and P. G. Ranjith, "Reuse of iron ore mineral wastes in civil engineering constructions: A case study," *Resources, Conservation and Recycling*, vol. 52, no. 11, pp. 1283–1289, 2008.

[58] J. R. Conner, *Chemical fixation and solidification of hazardous wastes*. Van Nostrand Reinhold New York, 1990.

[59] F. S. Hashem, M. S. Amin, and E. E. Hekal, "Stabilization of Cu (II) wastes by C3S hydrated matrix," *Construction and Building Materials*, vol. 25, no. 8, pp. 3278–3282, 2011.

[60] M. F. M. Zain, M. N. Islam, S. S. Radin, and S. G. Yap, "Cement-based solidification for the safe disposal of blasted copper slag," *Cement and Concrete Composites*, vol. 26, no. 7, pp. 845–851, 2004.

[61] H. Zhang, S. Mu, J. Cai, J. Liu, and J. Hong, "The role of iron in cement hydration process: From perspective of chemical admixture," *Thermochimica Acta*, vol. 722, p. 179457, 2023.

[62] M. A. Largeau, R. Mutuku, and J. Thuo, "Effect of Iron Powder (Fe 2 O 3) on Strength, Workability, and Porosity of the Binary Blended Concrete," *Open Journal of Civil Engineering*, vol. 8, no. 04, p. 411, 2018.

[63] Y. Yang, L. Chen, X. Sun, and Y. Mao, "Preparation of micro-iron ore tailings by wet-grinding and its application in sulphoaluminate cement," *Journal of Renewable Materials*, vol. 10, no. 4, p. 1007, 2022.

[64] E. Kapeluszna, Ł. Kotwica, and W. Nocuń-Wczelik, "Comparison of the effect of ground waste expanded perlite and silica fume on the hydration of cements with various tricalcium aluminate content – Comprehensive analysis," *Construction and Building Materials*, vol. 303, no. July, 2021, doi: 10.1016/j.conbuildmat.2021.124434.

[65] M. Hu, X. Zhu, and F. Long, "Alkali-activated fly ash-based geopolymers with zeolite or bentonite as additives," *Cement and Concrete Composites*, vol. 31, no. 10, pp. 762–768, 2009.

[66] H. Biricik and N. Sarier, "Comparative study of the characteristics of nano silica-, silica fume-and fly ash-incorporated cement mortars," *Materials Research*, vol. 17, pp. 570–582, 2014.

[67] K. Snehal, B. B. Das, and S. Barbhuiya, "Synergistic effect of nano silica on carbonation resistance of multi-blended cementitious mortar," *Cement and Concrete Composites*, vol. 141, p. 105125, 2023.

[68] L. Yu, Z. Zhang, X. Huang, B. Jiao, and D. Li, "Enhancement experiment on cementitious activity of copper-mine tailings in a geopolymer system," *Fibers*, vol. 5,

no. 4, p. 47, 2017.

[69] S. Ahmari, K. Parameswaran, and L. Zhang, "Alkali activation of copper mine tailings and low-calcium flash-furnace copper smelter slag," *Journal of materials in civil engineering*, vol. 27, no. 6, p. 4014193, 2015.

[70] I. C. Ferreira *et al.*, "Reuse of iron ore tailings for production of metakaolin-based geopolymers," *Journal of Materials Research and Technology*, vol. 18, pp. 4194–4200, 2022.

[71] A. Jagadisha, K. B. Rao, G. Nayak, and M. Kamath, "Influence of nano-silica on the microstructural and mechanical properties of high-performance concrete of containing EAF aggregate and processed quarry dust," *Construction and Building Materials*, vol. 304, p. 124392, 2021.

[72] A. Y. Patil *et al.*, "Multi-scale study on mechanical property and strength of new green sand (Poly Lactic Acid) as replacement of fine aggregate in concrete mix," *Symmetry*, vol. 12, no. 11, p. 1823, 2020.

[73] Q. Hu *et al.*, "Direct three-dimensional observation of the microstructure and chemistry of C3S hydration," *Cement and concrete research*, vol. 88, pp. 157–169, 2016.

[74] E. P. Sumukh, S. K. Goudar, and B. B. Das, "Predicting the Service Life of Reinforced Concrete by Incorporating the Experimentally Determined Properties of Steel–Concrete Interface and Corrosion BT - Recent Trends in Civil Engineering," 2021, pp. 399–417.

[75] E. P. Sumukh, S. K. Goudar, and B. B. Das, *A Review on the Properties of Steel-Concrete Interface and Characterization Methods*, vol. 78. 2021. doi: 10.1007/978-981-15-5001-0_15.

[76] S. K. Goudar, E. P. Sumukh, and B. B. Das, "Influence Of Marine Environment Exposure On The Engineering Properties Of Steel-concrete Interface," *The Open Civil Engineering Journal*, vol. 16, no. 1, 2022.

Figure Captions:

Fig. 1. a) Particle size distribution of various materials used, b) Mineralogical composition of fine aggregates used

Fig. 2. a) Mine tailing, b) scanning electron micrograph at 500X, c) scanning electron micrograph at 10,000X

Fig. 3. Particle packing curves of a) IOT based mortars and b) COT based mortars determined using modified Andreasen and Andersen particle packing model

Fig. 4. a) Flow characteristics of a) IOT based mortar; b) COT based mortar

Fig. 5. a) Compressive strength, c) Water absorption, e) permeable porosity of IOT based mortars, and b) Compressive strength, d) Water absorption, f) Permeable porosity of COT based mortars

Fig. 6. XRD pattern of optimized mortars at the curing age of a) 28 days and b) 120 days

Fig. 7. TG and DTG curves of a) IOT based mortar after 28 days of curing, b) IOT based mortar after 120 days of curing, c) COT based mortar after 28 days of curing and d) COT based mortar after 120 days of curing

Fig. 8. Phase compounds formed in IOT based mortar [(a) CH; (c) CC] and COT based mortar [(b) CH; (d) CC] after 28 days and 120 days of curing

Fig. 9. FTIR spectra of control and IOT based mortar samples at a) 28 days of curing and b) 120 days of curing

Fig. 10. FTIR spectra of control and COT based mortar samples at a) 28 days of curing and b) 120 days of curing

Fig. 11. Scanning electron micrograph of control (CM) [in a), b)], I20 [in c), d)] and C30 [in e), f)] mortar at 28 days of curing.

Fig. 12. Scanning electron micrograph of control (CM) [in a), b)], I20 [in c), d)] and C30 [in e), f)] mortar at 120 days of curing.